J. Fluid Mech. (1985), *vol.* 160, *pp.* 93–117
Printed in Great Britain

Numerical solution of the early stage of the unsteady viscous flow around a circular cylinder: a comparison with experimental visualization and measurements

By TA PHUOC LOC
LIMSI–CNRS, B.P. 30, 91406 Orsay, France
AND R. BOUARD
Laboratoire de Mécanique des Fluides, Université de Poitiers, 86022 Poitiers, France

(Received 25 October 1984 and in revised form 7 May 1985)

Early stages of unsteady viscous flows around a circular cylinder at Reynolds numbers of 3×10^3 and 9.5×10^3 are analysed numerically by direct integration of the Navier–Stokes equations – a fourth-order finite-difference scheme is used for the resolution of the stream-function equation and a second-order one for the vorticity-transport equation. Evolution with time of the flow structure is studied in detail. Some new phenomena are revealed and confirmed by experiments.

The influence of the grid systems and the downstream boundary conditions on the flow structure and the velocity profiles is reported. The computed results are compared qualitatively and quantitatively with experimental visualization and measurements. The comparison is found to be satisfactory.

1. Introduction

The time development of an incompressible viscous flow induced by an impulsively started circular cylinder is a classical problem in fluid mechanics. Despite the simplicity of the obstacle geometry, the flow structure is complex and all the phenomena of fluid mechanics are present. That is why, for more than a century, numerous theoretical, numerical and experimental investigations have been reported in the literature.

Theoretical works concerning the unsteady flow around an impulsively started circular cylinder are generally based on boundary-layer theory. Blasius (1908), Goldstein & Rosenhead (1936), Schuh (1953), Wundt (1955) and Watson (1955) have all considered this problem in the limiting case of infinite Reynolds number. Some authors (Wang 1967; Collins & Dennis 1973*a*, *b*) have extended their work to finite but high Reynolds numbers. The results are only available for short spans of time after the starting.

Purely numerical solutions of the unsteady Navier–Stokes equations have also been developed and applied to this problem. These are, on the whole, valid for any value of the Reynolds number. However, no results for Reynolds numbers greater than 2000 have previously been obtained numerically and compared satisfactorily with experimental visualization.

The first numerical solution of unsteady flow around a circular cylinder was given by Payne (1958) for Reynolds numbers of 40 and 100. Other investigations were

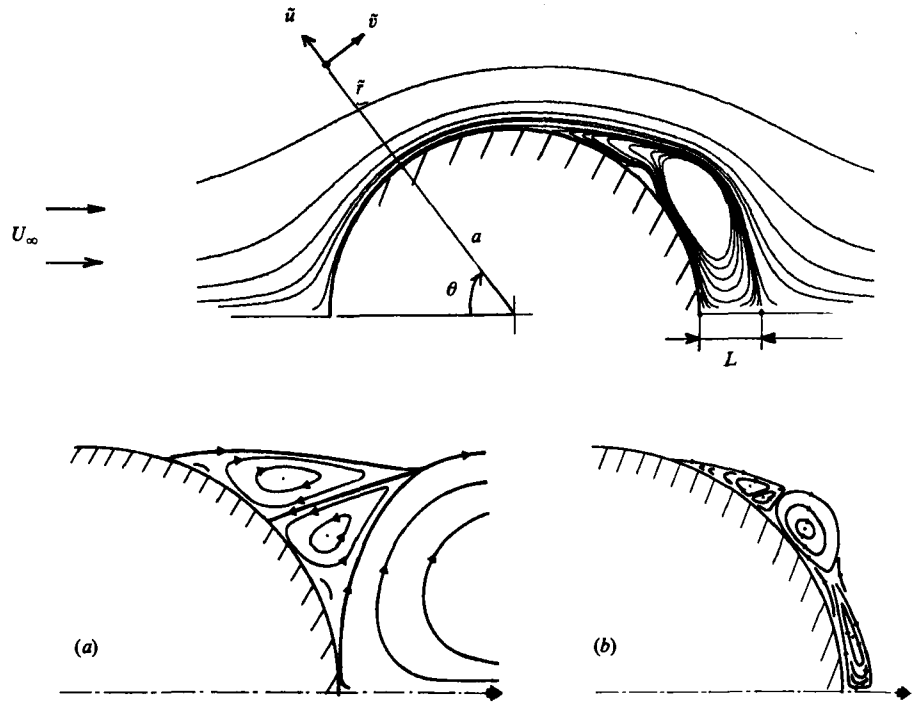

FIGURE 1. Schematic of the physical problem: (*a*) phenomenon α; (*b*) phenomenon β.

proposed by Kawaguti & Jain (1966), Ingham (1968), Son & Hanratty (1969), Jain & Rao (1969), Thoman & Szewczyk (1969), Dennis & Staniforth (1971), Patel (1976) and Daube & Ta Phuoc Loc (1978). The common points of interest of these works are the development of the main unsteady wake length behind the cylinder, and the time evolutions of the drag coefficient and of the separation angle. An attempt to analyse secondary-vortex formation has been presented by Ta Phuoc Loc (1980) for Reynolds numbers up to 1000.

Besides these theoretical and numerical investigations, some experimental visualizations were described by Honji & Taneda (1969), Taneda (1972) and Coutanceau & Bouard (1977, 1979). The phenomena of the formation and the development of the main and secondary vortices have been studied qualitatively and quantitatively in detail by Bouard & Coutanceau (1980) for Reynolds numbers up to 10^4.

Several comparisons between experimental data and numerical or theoretical results have been carried out, and they show good agreement for Reynolds numbers up to 10^3. A discrepancy exists for greater Reynolds numbers, especially at the first moment of the starting.

The aim of the present paper is to analyse the flow structure at early times of the impulsively started circular cylinder at Reynolds numbers of 3×10^3 and 9.5×10^3, which are values for which experimental data exist. The phenomenon β of 'forewake' (figure 1) detected by visualization at $Re = 9.5 \times 10^3$ by Bouard & Coutanceau (1980) is found in numerical simulation at the same instant. The secondary vortices, which are stable and confined in the main wake for $Re < 10^3$, become unstable for greater Reynolds numbers. They interact alternatively with the external main flow and the primary wake for $Re = 9.5 \times 10^3$. This phenomenon is brought out by numerical simulation and confirmed by experimental visualization. To ensure the validity of

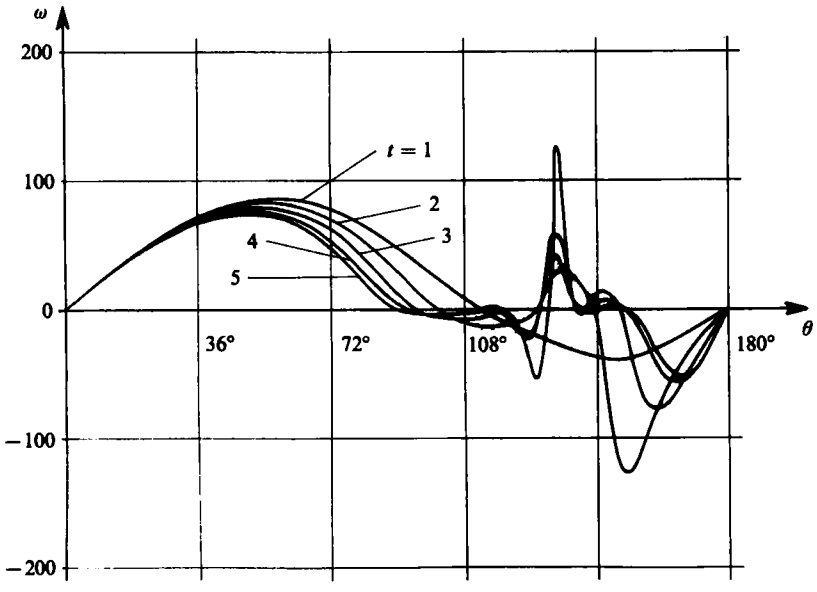

FIGURE 2. Evolution with time of the vorticity repartition on the surface of the cylinder for $Re = 3000$.

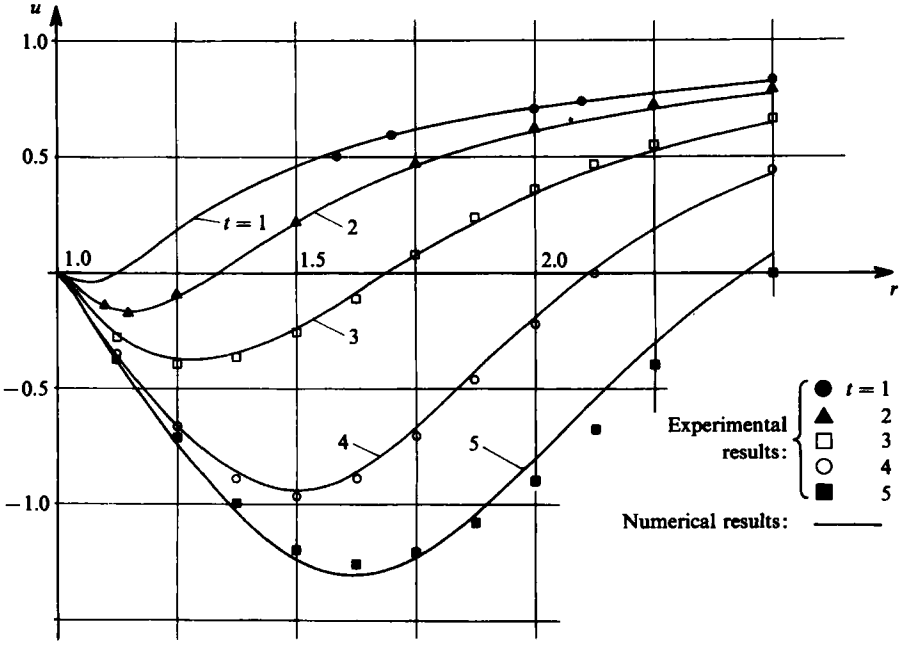

FIGURE 3. Comparison between experimental and numerical results for the velocity profile for $Re = 3000$.

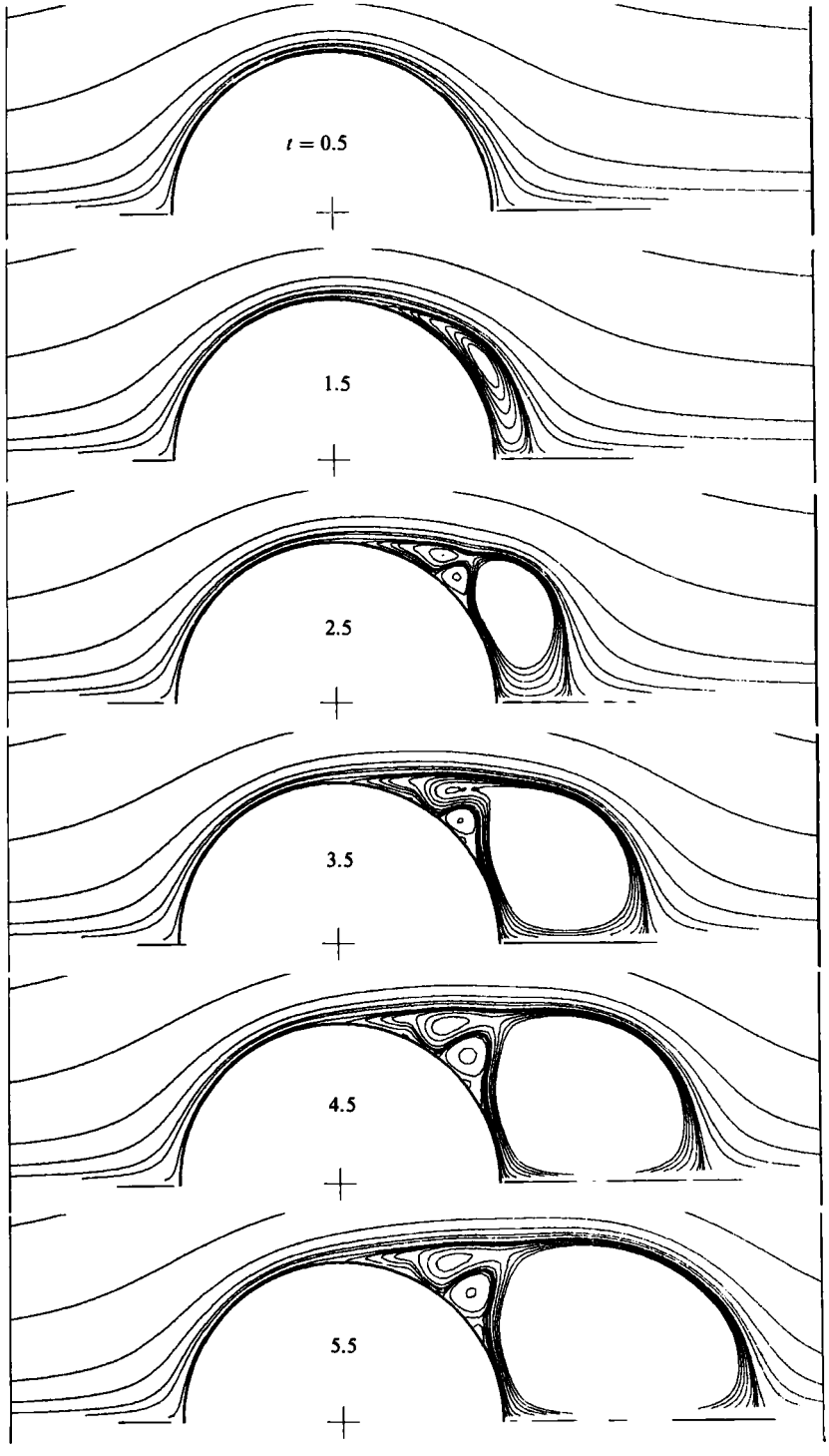

FIGURE 4. Evolution with time of the flow structure for $Re = 3000$.

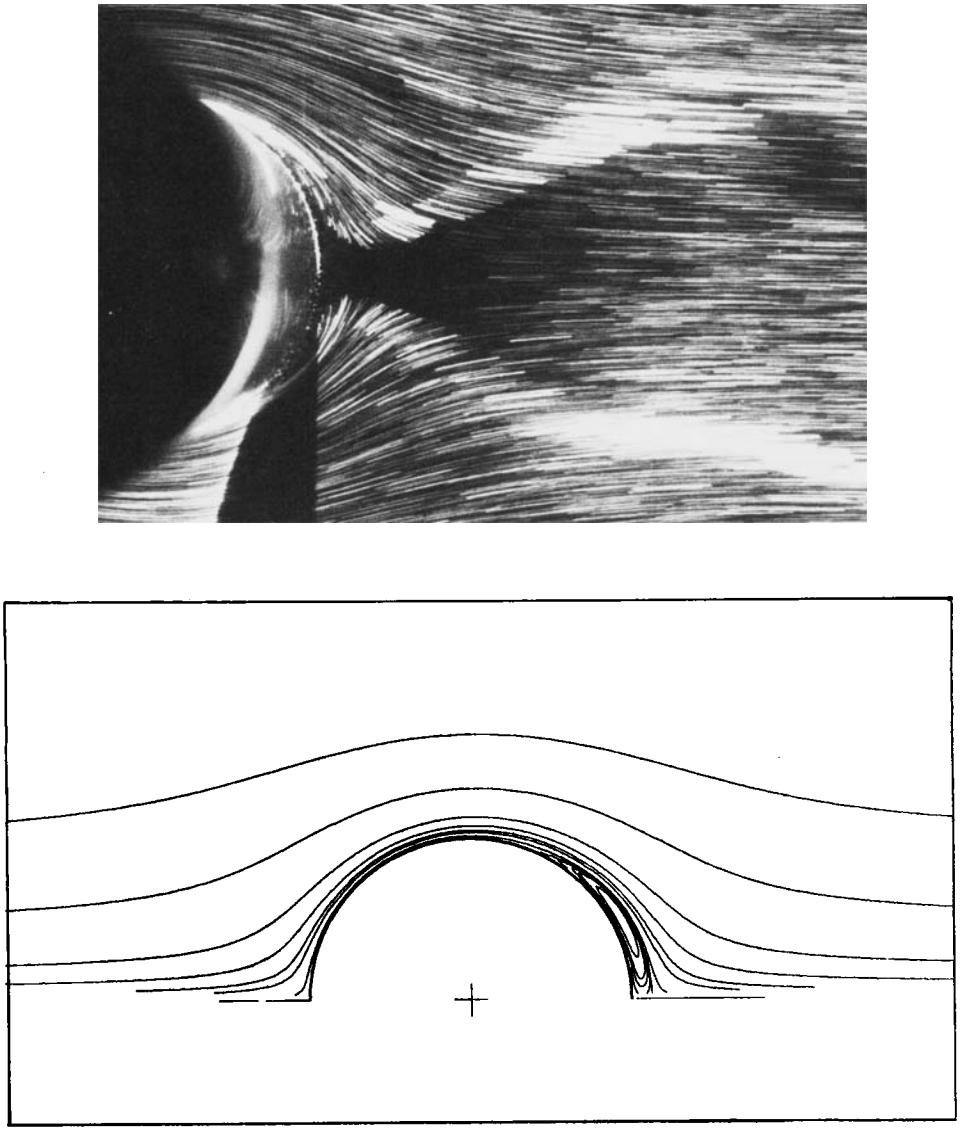

FIGURE 5. Comparison of the flow structure obtained by experimental visualization and by numerical simulation for $Re = 3000$; $t = 1$.

numerical results, two grid-systems have been used for a Reynolds number of 9.5×10^3.

All the computations given in this paper are compared with experimental visualization.

2. Basic equations

In stream-function and vorticity formulation the unsteady Navier–Stokes equations can be written as

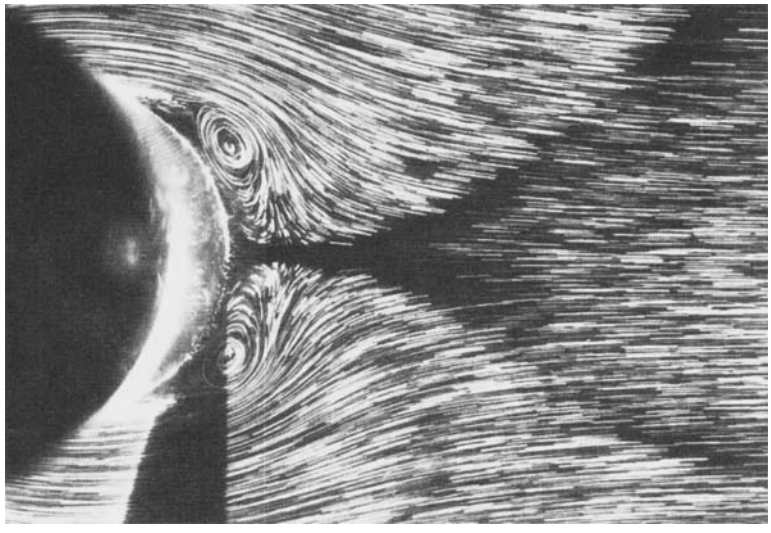

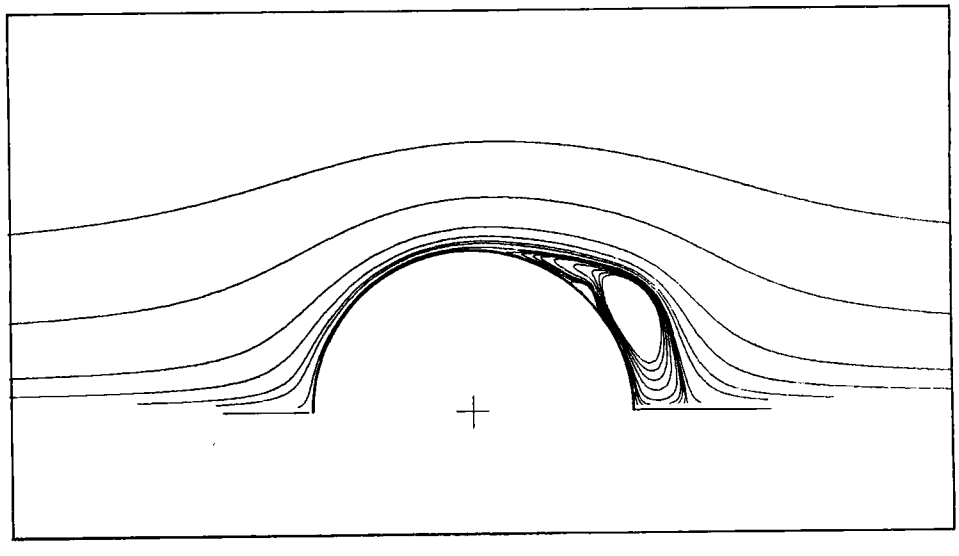

FIGURE 6. As figure 5; $t = 2$.

$$\frac{\partial\tilde{\omega}}{\partial\tilde{t}}-\frac{1}{\tilde{r}}\left(\frac{\partial}{\partial\tilde{r}}\left(\tilde{\omega}\frac{\partial\tilde{\psi}}{\partial\theta}\right)-\frac{\partial}{\partial\theta}\left(\tilde{\omega}\frac{\partial\tilde{\psi}}{\partial\tilde{r}}\right)\right)=\nu\nabla^2\tilde{\omega}, \tag{1}$$

$$\tilde{\omega}=\nabla^2\tilde{\psi}, \tag{2}$$

with

$$\nabla^2=\frac{\partial^2}{\partial\tilde{r}^2}+\frac{1}{\tilde{r}}\frac{\partial}{\partial\tilde{r}}+\frac{1}{\tilde{r}^2}\frac{\partial^2}{\partial\theta^2},$$

where $(\tilde{r}, \theta)$ are polar coordinates, ν is the kinematic viscosity and $\tilde{t}$ the time. The variables $\tilde{\psi}$ and $\tilde{\omega}$ are defined by

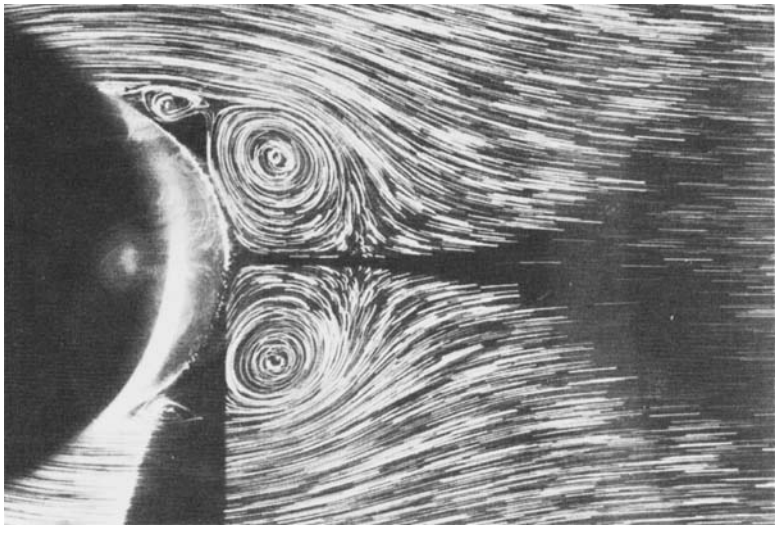

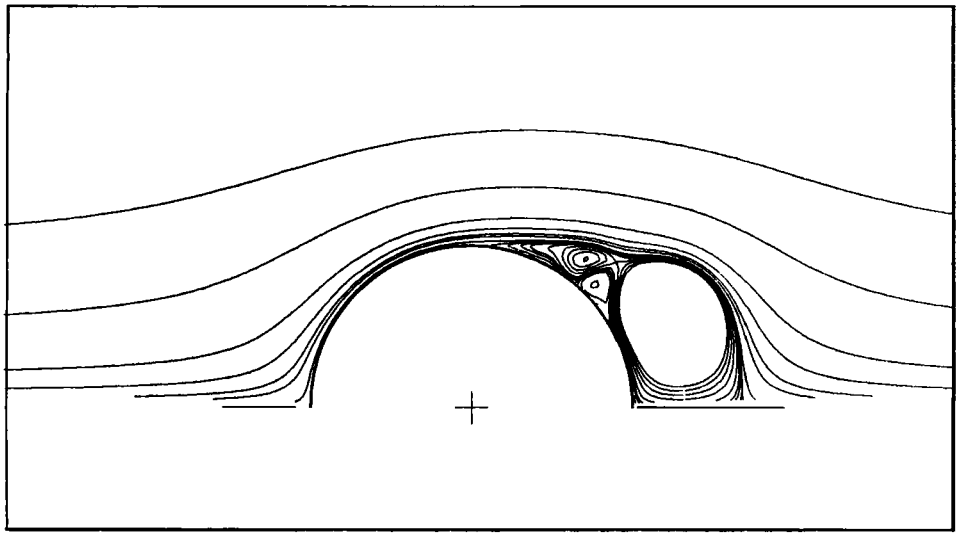

FIGURE 7. As figure 5; $t = 3$.

$$\tilde{u} = -\frac{1}{\tilde{r}}\frac{\partial \tilde{\psi}}{\partial \theta}, \quad \tilde{v} = \frac{\partial \tilde{\psi}}{\partial \tilde{r}},$$

$$\tilde{\omega} = \frac{1}{\tilde{r}}\left(\frac{\partial}{\partial \tilde{r}}(\tilde{v}\tilde{r}) - \frac{\partial \tilde{u}}{\partial \theta}\right).$$

If we write

$$r = \frac{\tilde{r}}{a} = e^{\pi\xi}, \quad \theta = \pi\eta, \quad D = 2a,$$

$$Re = \frac{2U_\infty a}{\nu}, \quad t = \frac{\tilde{t}}{a}u_\infty,$$

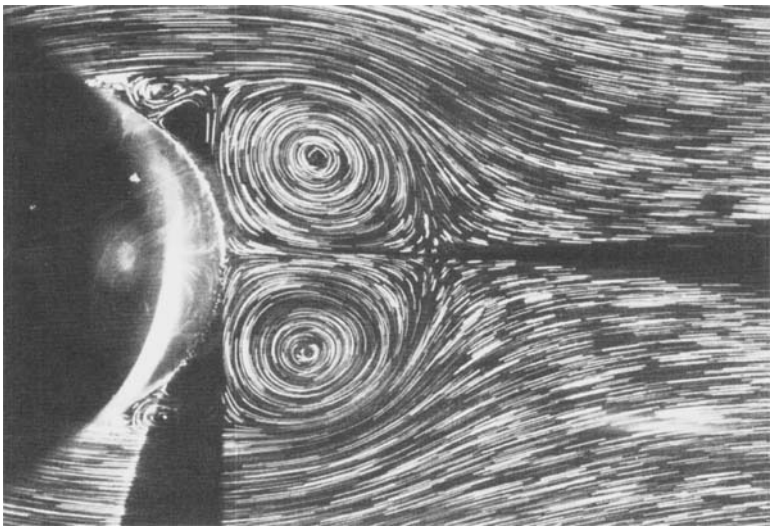

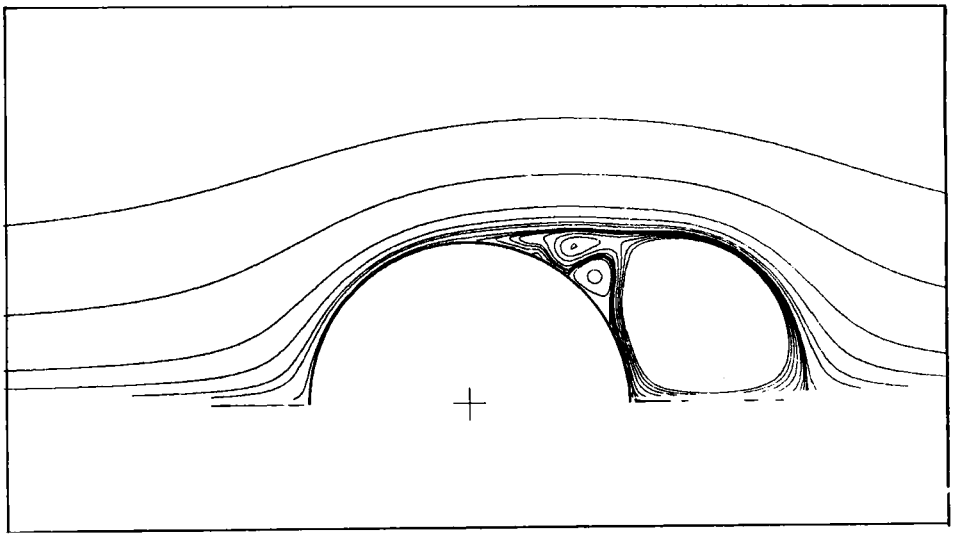

FIGURE 8. As figure 5; $t = 4$.

$$\psi = \frac{\tilde{\psi}}{u_\infty a}, \quad \omega = \frac{\tilde{\omega} a}{u_\infty},$$

then (1) and (2) become, in dimensionless form,

$$\frac{Re}{2}\left[g(\xi,\eta)\frac{\partial\omega}{\partial t}+\frac{\partial}{\partial\eta}\left(\frac{\partial\psi}{\partial\xi}\omega\right)-\frac{\partial}{\partial\xi}\left(\frac{\partial\psi}{\partial\eta}\omega\right)\right] = \nabla^2\omega, \tag{3}$$

$$\nabla^2\psi = g(\xi,\eta)\,\omega, \tag{4}$$

with

$$\nabla^2 = \frac{\partial^2}{\partial\xi^2}+\frac{\partial^2}{\partial\eta^2}, \quad g(\xi,\eta) = \pi^2\,\mathrm{e}^{2\pi\xi}.$$

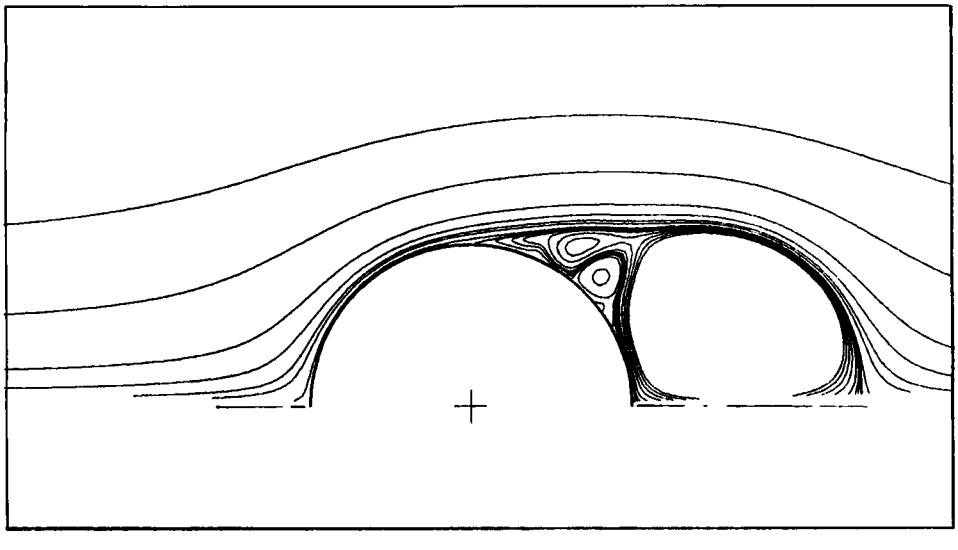

FIGURE 9. As figure 5; $t = 5$.

3. Boundary and initial conditions – numerical method

3.1. *Boundary and initial conditions*

To complete the equations (3) and (4), the boundary and initial conditions of the physical problem are

(i) no slip on the surface of the cylinder;
(ii) uniform flow at infinity;
(iii) initially, the cylinder at rest in the fluid.

These conditions can be written in stream-function and vorticity formulation as

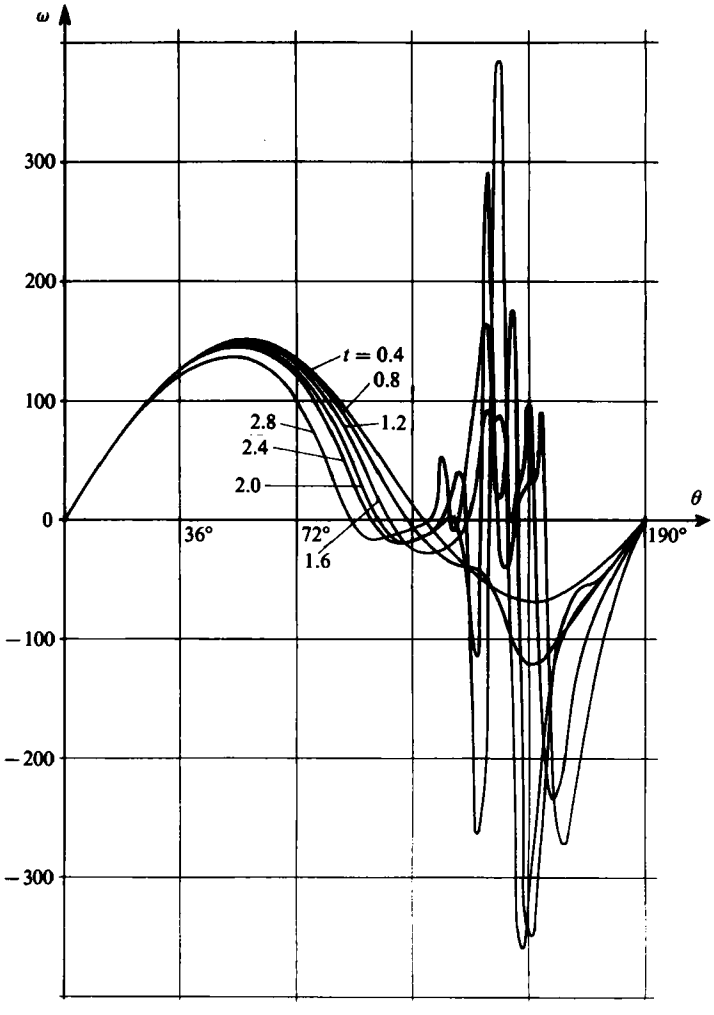

FIGURE 10. Evolution with time of the vorticity repartition on the surface of the cylinder for $Re = 9500$.

$$\left.\begin{aligned} &\psi = 2\sinh\pi\xi\sin\pi\eta, \\ &\omega = 0 \end{aligned}\right\} \quad (\xi \to \infty);$$

$$\left.\begin{aligned} &\psi = \frac{\partial\psi}{\partial\xi} = 0, \\ &\text{no condition on } \omega \end{aligned}\right\} \quad (\xi = 0),$$

for $t \geqslant 0$.

Equation (4) gives also

$$\frac{\partial^2\psi}{\partial\xi^2} = g(\xi, \eta)\,\omega \quad (\xi = 0).$$

This condition is necessary in the fourth-order compact numerical algorithm, and allows us to determine the boundary value for ω at the surface of the cylinder.

Unlike Collins & Dennis (1973), who use the boundary-layer solution as the initial conditions in their truncation-series method, we have chosen, in our studies, the

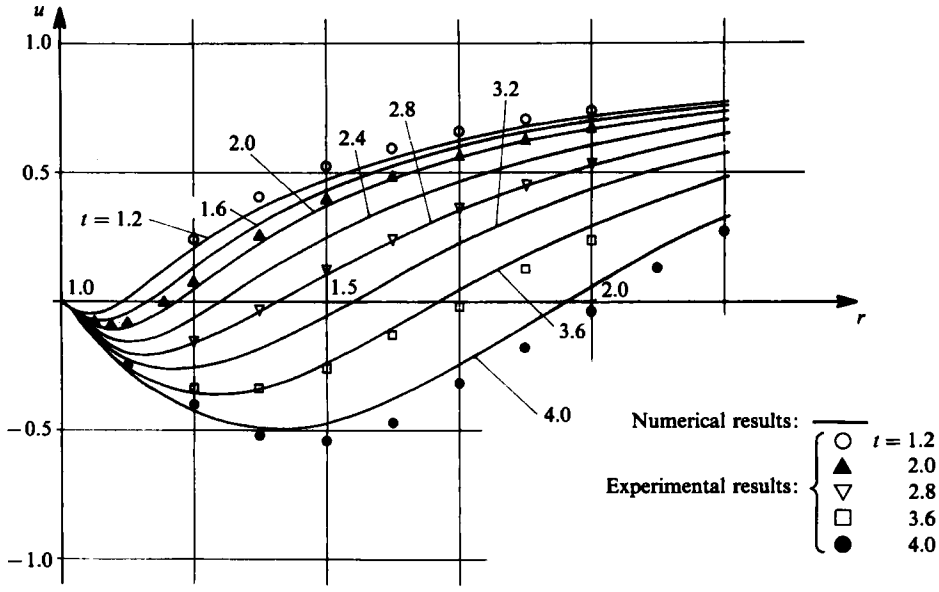

FIGURE 11. Comparison between experimental and numerical results for the velocity profile for $Re = 9500$.

steady solution of very low Reynolds number ($Re = 5$) of the Navier–Stokes equations as initial conditions. This choice is justified by experimental observations, and is consistent with the Navier–Stokes equations. The starting movement is obtained with an abrupt change of Reynolds number.

In fact, in the problem of unsteady flow around a circular cylinder fitted with an attached flap, for which there does not exist any analytical boundary-layer solution, we have considered two classes of initial conditions. First, the flow is assumed to be initially irrotational with or without the Kutta–Joukowski condition. Secondly, the flow is supposed to be in the Stokes regime, and a solution of the Navier–Stokes equations for very low Reynolds number gives the initial conditions. Our numerical results have been compared with the experimental visualization carried out by the Laboratoire de Mécanique des Fluides de Poitiers. From this comparison it can be stated that the second class of the initial conditions is the only solution that reproduces correctly the flow structure and the starting vortex. This procedure has shown excellent agreement in space and time between numerical and experimental results.

3.2. *Numerical method*

Details of the numerical scheme have been clearly explained in Ta Phuoc Loc (1980). It is a finite-difference method, which uses a fourth-order compact scheme to solve the stream-function Poisson equation and a classic second-order one for the transport equation of the vorticity. The divergence form of the convection terms is considered with a second-order discretized formula.

This method was also applied successfully to the problem of the stall around an airfoil by Monnet *et al.* (1983).

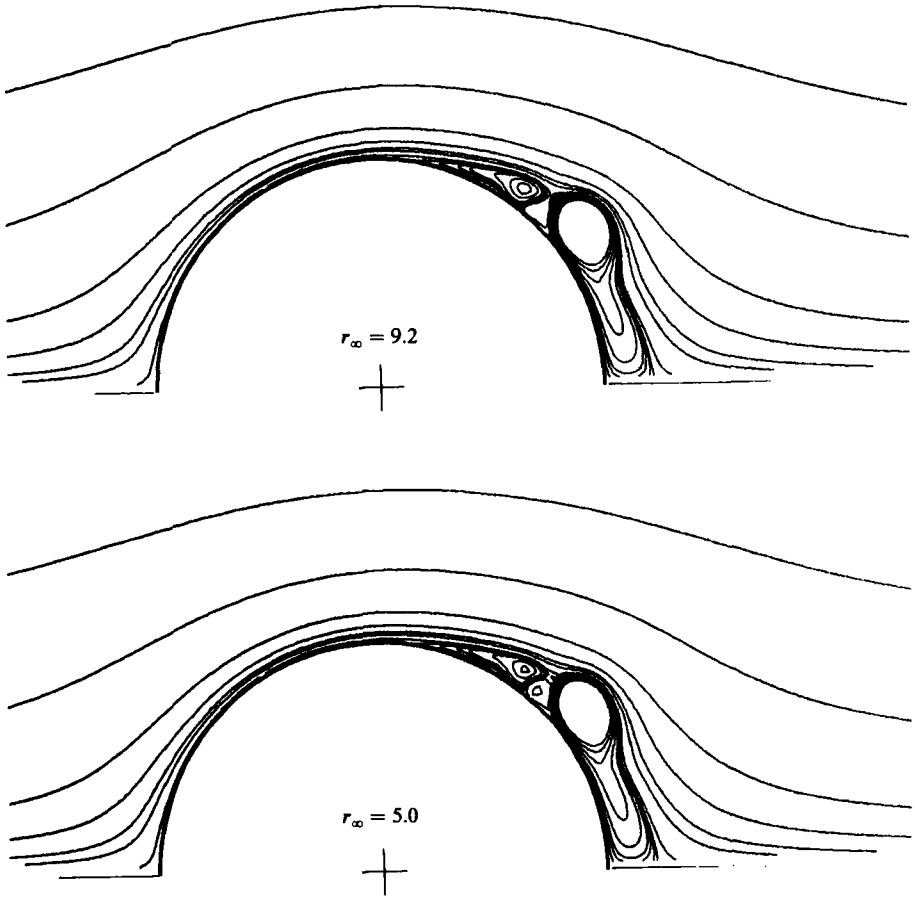

(*a*)

FIGURE 12(*a*). For caption see facing page.

4. Results

The numerical calculations have been made on a NAS 9080 computer. For a Reynolds number of 9500 two values of r_∞ and two types of boundary conditions at 'infinity' are considered. At the first stage the irrotational flow has been imposed at this downstream boundary. At the second stage we have imposed an open boundary condition for the downstream flow. The domain of calculation is limited to $0 \leqslant \theta \leqslant \pi$ because of the symmetry of the phenomenon at the initial moment of the starting.

4.1. $Re = 3000$

In Ta Phuoc Loc (1980) it was shown, by numerical simulation, that secondary vortices appear for Reynolds numbers up to 1000. A pair of secondary vortices (phenomenon α) (figure 1) is only apparent at $Re = 1000$. To confirm this flow structure, we consider here a calculation corresponding to $Re = 3000$, a value for which experimental visualizations and measurements have been obtained by Bouard & Coutanceau (1980).

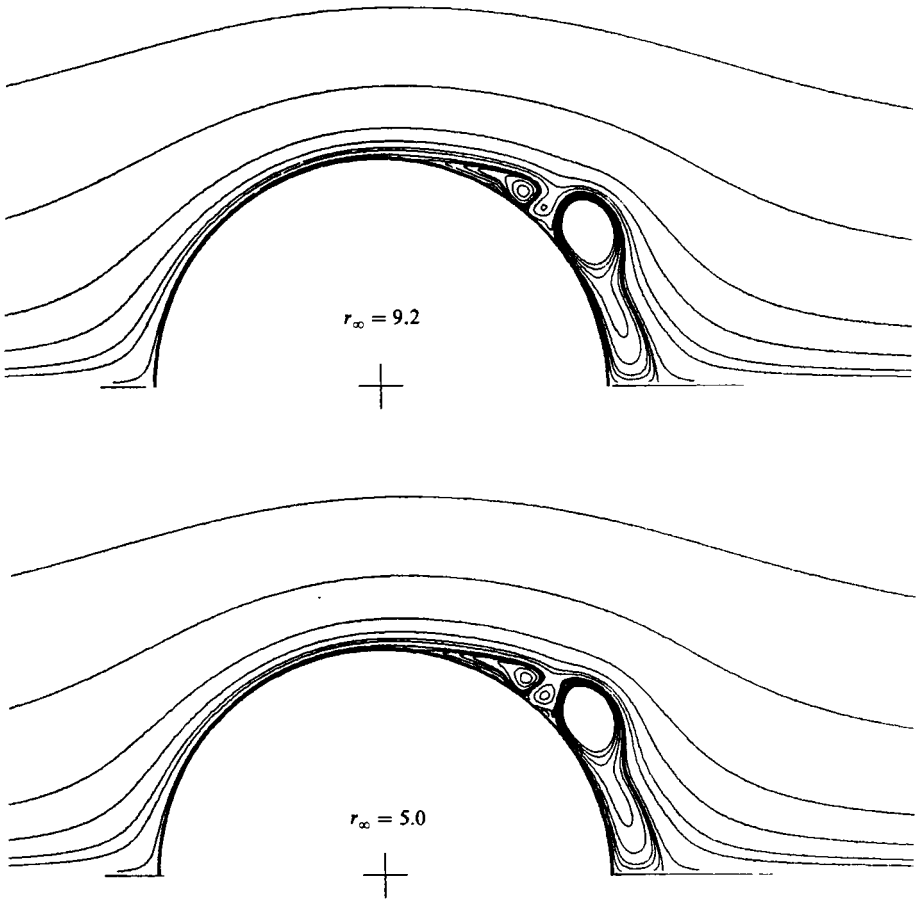

FIGURE 12. Influence of the grid system and of the domain of calculation on the flow structure: (*a*) 101 × 301 nodes; (*b*) 201 × 301 nodes.

For this Reynolds number a grid system of 101 × 141 nodes has been chosen. The physical domain is limited by $1 \leqslant r \leqslant 10$ and $0 \leqslant \theta \leqslant \pi$. The dimensionless time step is taken as 0.02. Irrotational flow has been imposed at the downstream boundary. The third-order-accurate formula has been used to calculate the vorticity at the surface of the cylinder.

The evolution with time of the vorticity distribution at the surface of the cylinder is reported in figure 2. The quantitative comparison (figure 3) for the radial velocity on the symmetry axis behind the cylinder shows good agreement between experimental data and computational results. We can see the existence of values of velocity modulus greater than 1 in the primary vortex. However, this maximum modulus of the velocity in the wake decreases when the Reynolds number increases from 1000 to 9500. Flow patterns at different times are shown in figure 4, showing the growth of primary and secondary vortices. At this Reynolds number, secondary vortices are always confined in the main wake and do not communicate with external flow. In figures 5–9 comparisons of the flow structure at $t = 1$, 2, 3, 4 and 5, given by experimental visualization and numerical simulation, are found satisfactory. All the

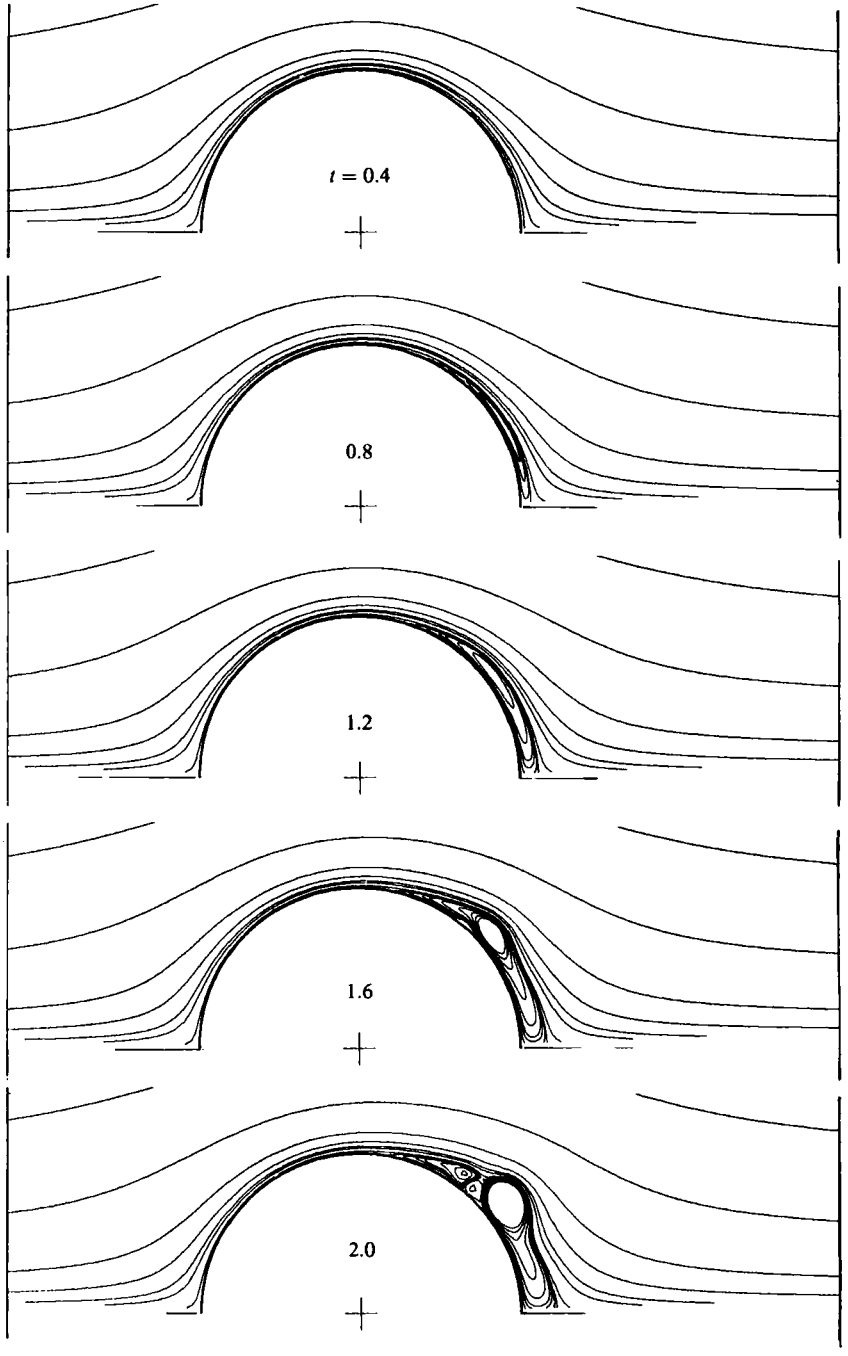

13

FIGURE 13. Evolution with time of the flow structure for $Re = 9500$; $t = 0.4$–2.0.

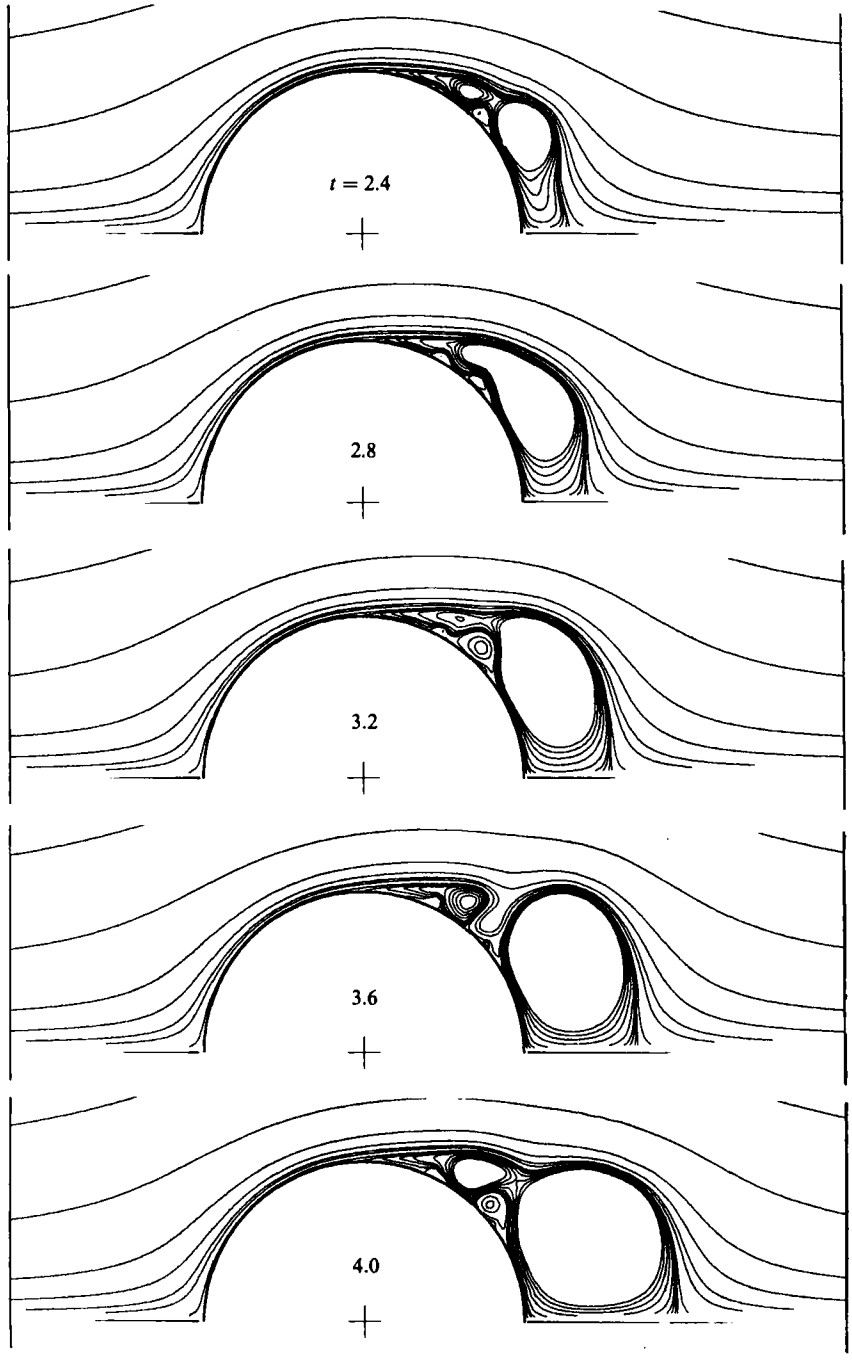

14

FIGURE 14. As figure 13; $t = 2.4$–4.0.

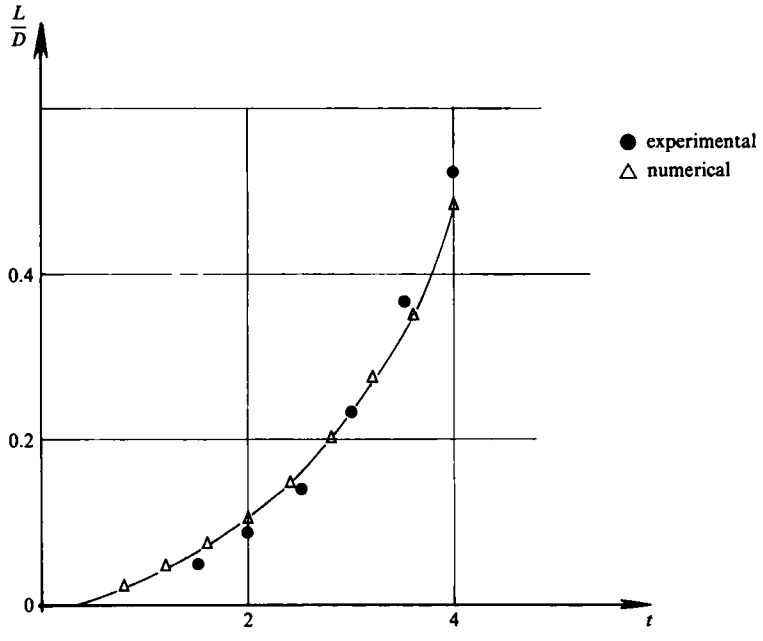

FIGURE 15. Comparison between experimental and numerical results on the unsteady main-wake length.

details of the flow pattern observed in visualization have been pointed out by computational treatment of the unsteady Navier–Stokes equations. We have demonstrated that the phenomenon α can be clearly exhibited by a numerical simulation and that it is much more accentuated than for Reynolds number equal to 1000.

4.2. $Re = 9500$

In Bouard & Coutanceau (1980) two main phenomena have been observed for Reynolds numbers greater than 500: the phenomenon α, which is visible from $Re = 1000$; and the phenomenon β (figure 1), observed at a very early phase of the flow establishment only for Reynolds numbers greater than 3000. Our purpose in this part is to analyse the phenomenon β numerically with sufficient accuracy. The formation and the stability of the so-called 'forewake' will be examined. For these reasons, the influence of different parameters such as the boundary conditions, the mesh size and the computation domain on the numerical results have also been considered.

Two values of the mesh size and two domains of computation ($r_\infty = 5$; $r_\infty = 9.2$) have been chosen for all calculations. The boundary conditions for the vorticity at the surface of the cylinder have been developed with second-order- or third-order-accurate formulas:

$$2g(0,\eta)\,\omega(0,\eta)+g(\Delta\xi,\eta)\,\omega(\Delta\xi,\eta)=\frac{6}{(\Delta\xi)^2}(\psi(\Delta\xi,\eta)-\psi(0,\eta))+O((\Delta\xi)^2),$$

$$g(0,\eta)\,\omega(0,\eta)=\frac{12}{(\Delta\xi)^2}\psi(\Delta\xi,\eta)-\frac{6}{\Delta\xi}\frac{\partial\psi}{\partial\xi}(\Delta\xi,\eta)+\frac{\partial^2\psi}{\partial\xi^2}(\Delta\xi,\eta)+O((\Delta\xi)^3).$$

Numerical results obtained with these two boundary-condition formulas have shown a negligible influence of the mesh size used.

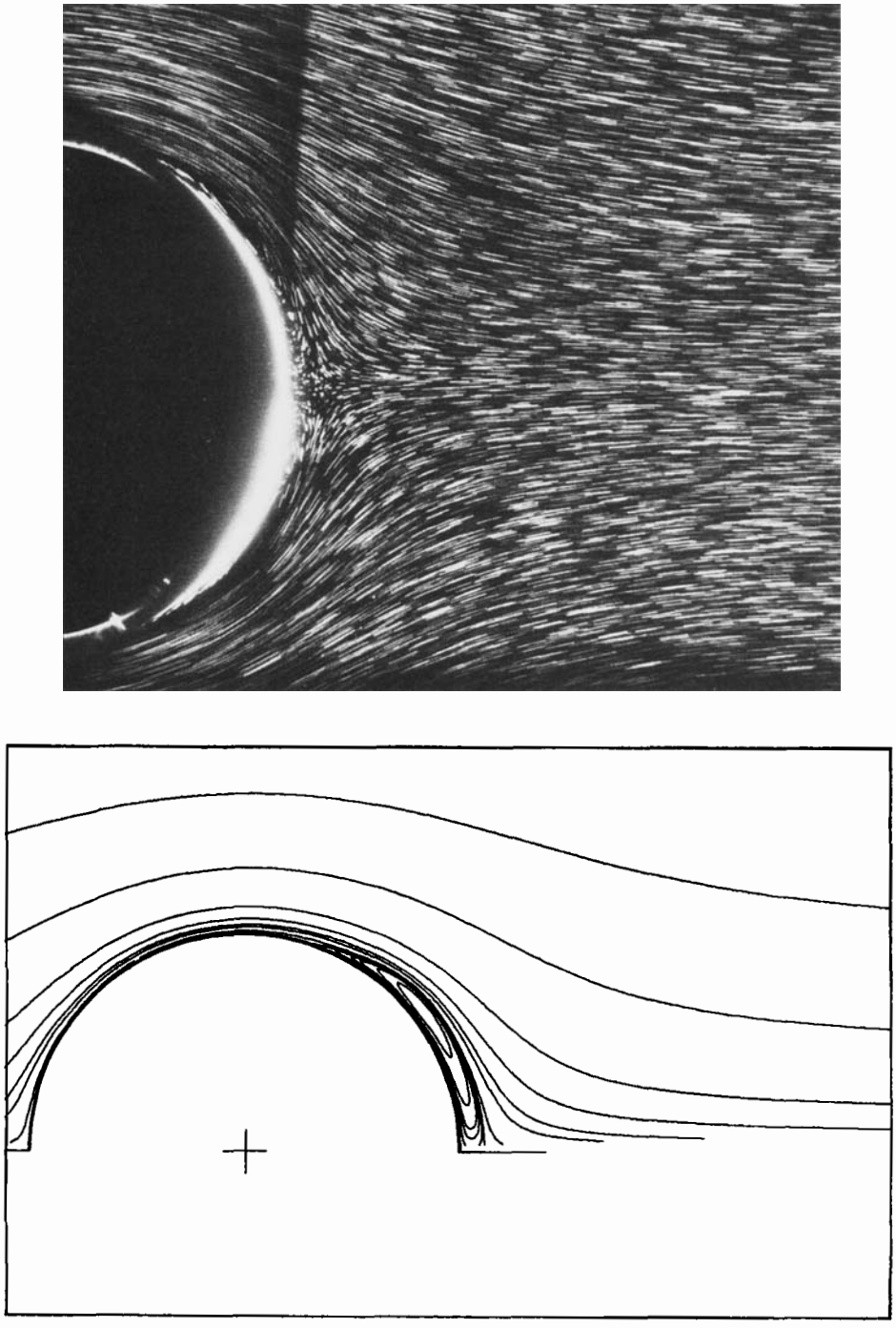

FIGURE 16. Comparison of the flow structure obtained by experimental visualization and by numerical simulation for $Re = 9500$; $t = 1.2$.

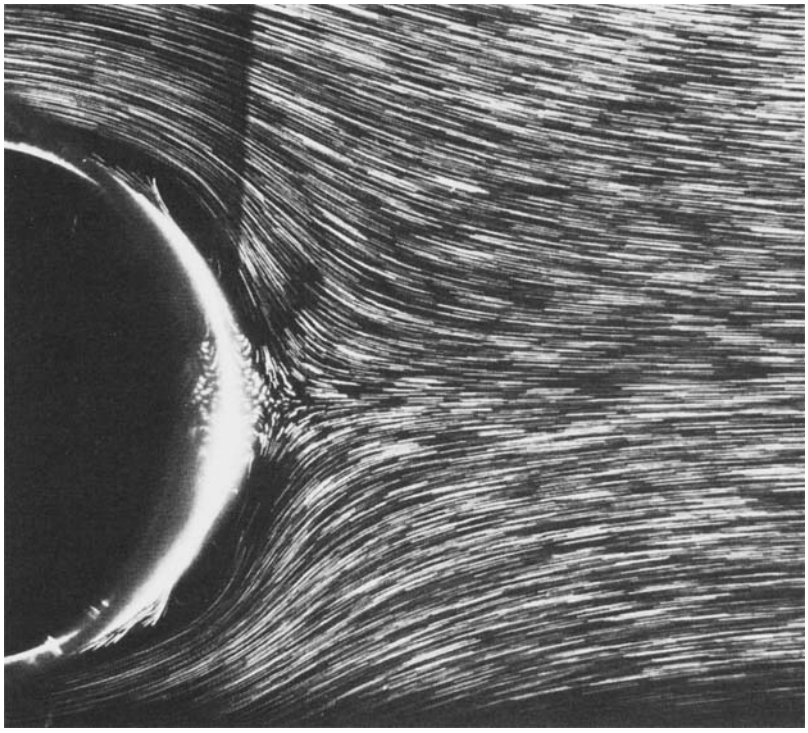

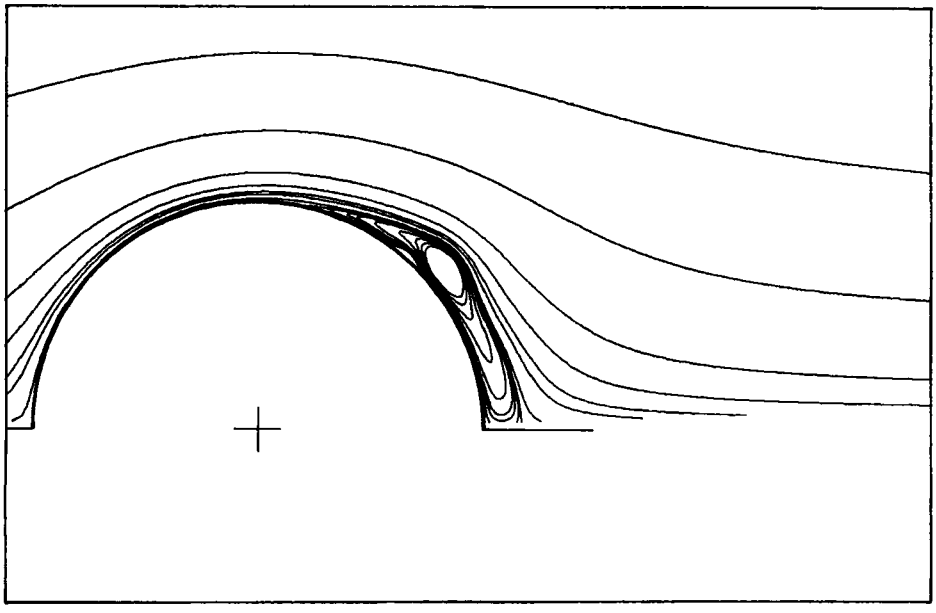

FIGURE 17. As figure 16; $t = 1.6$.

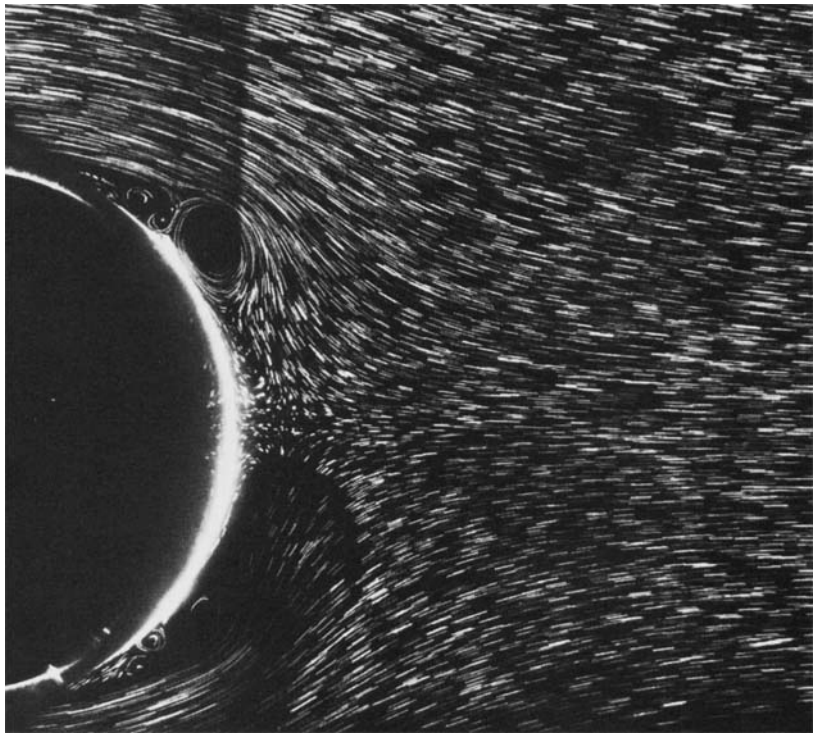

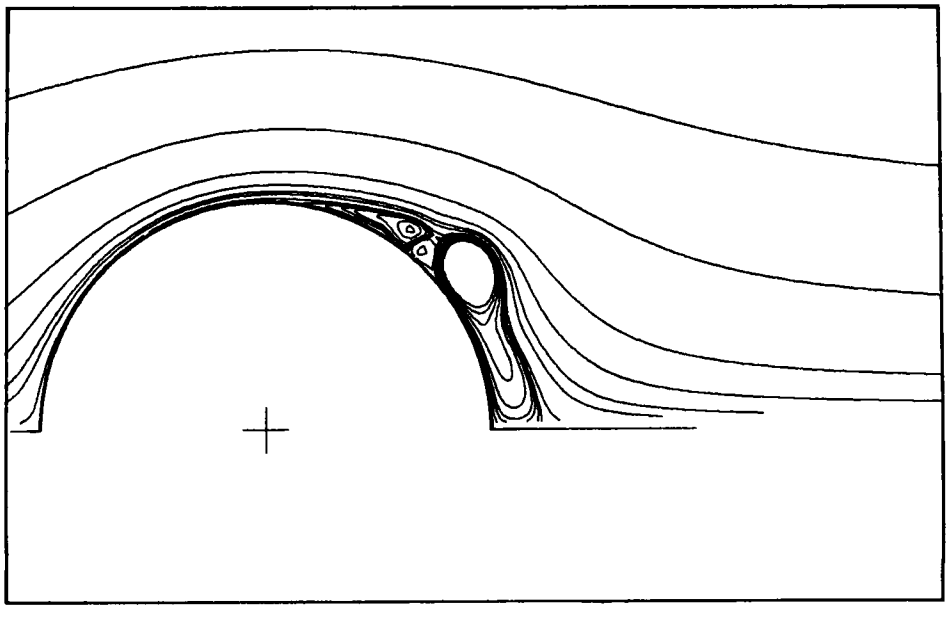

FIGURE 18. As figure 16; $t = 2$.

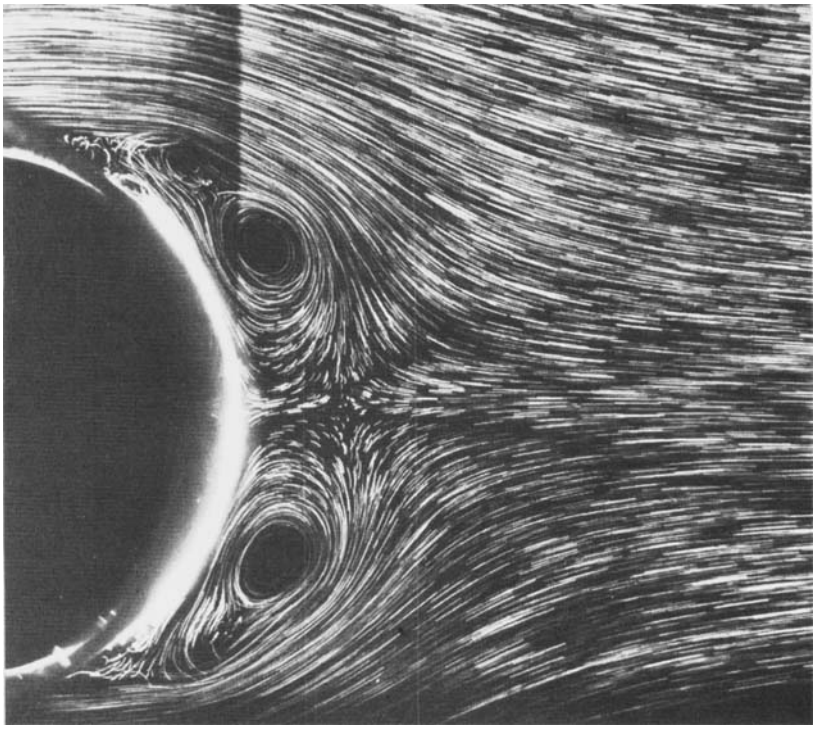

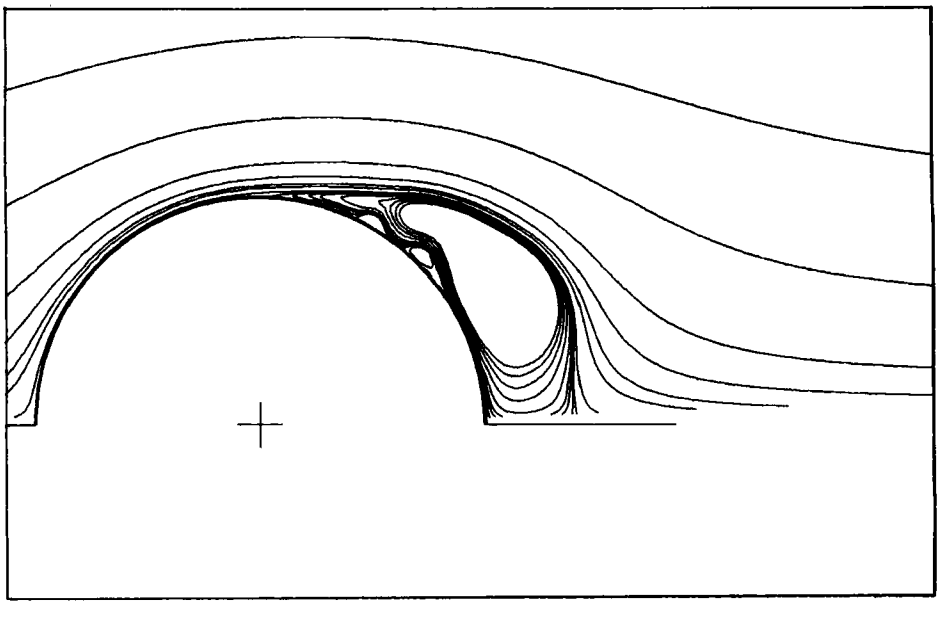

FIGURE 19. As figure 16; $t = 2.8$.

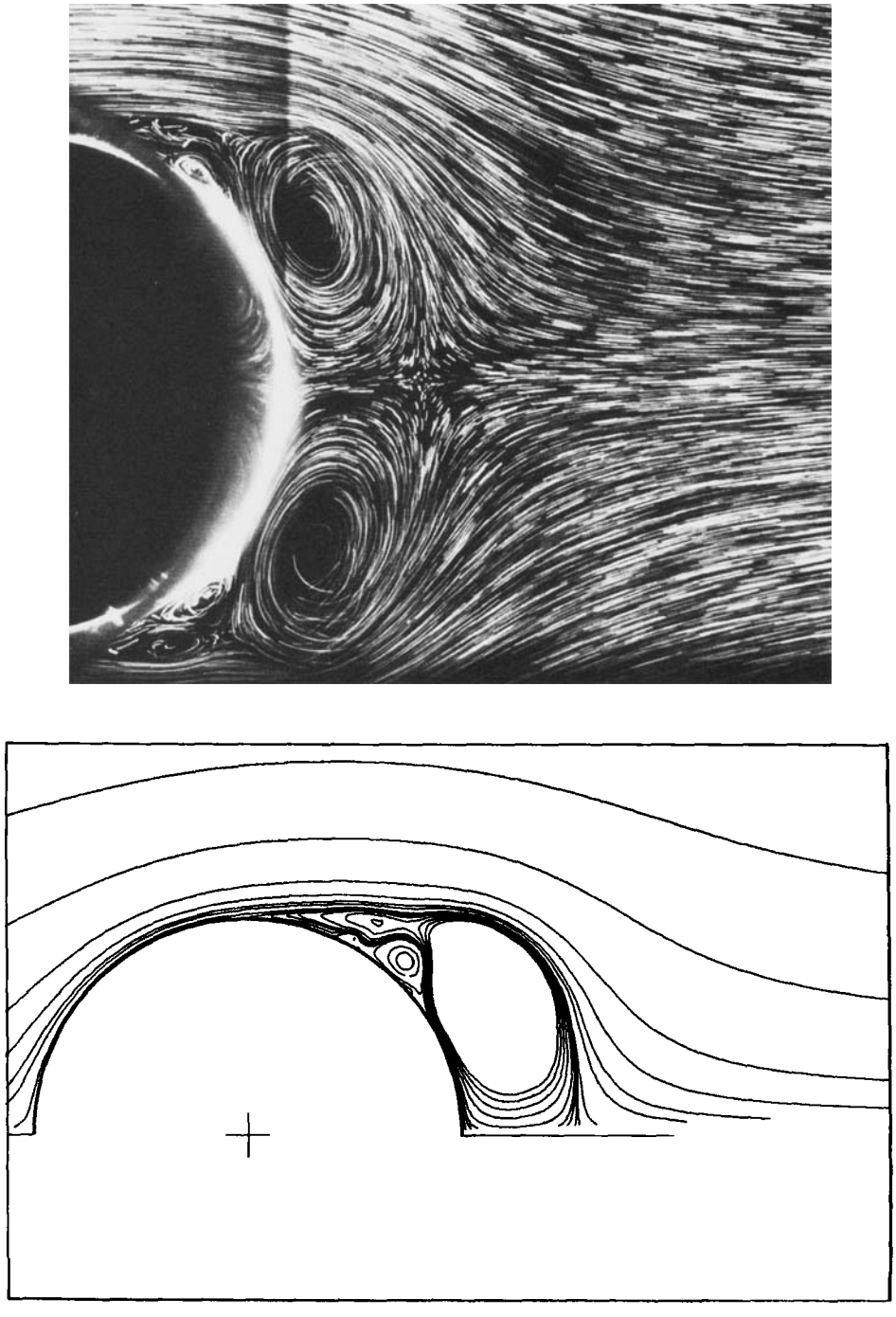

FIGURE 20. As figure 16; $t = 3.2$.

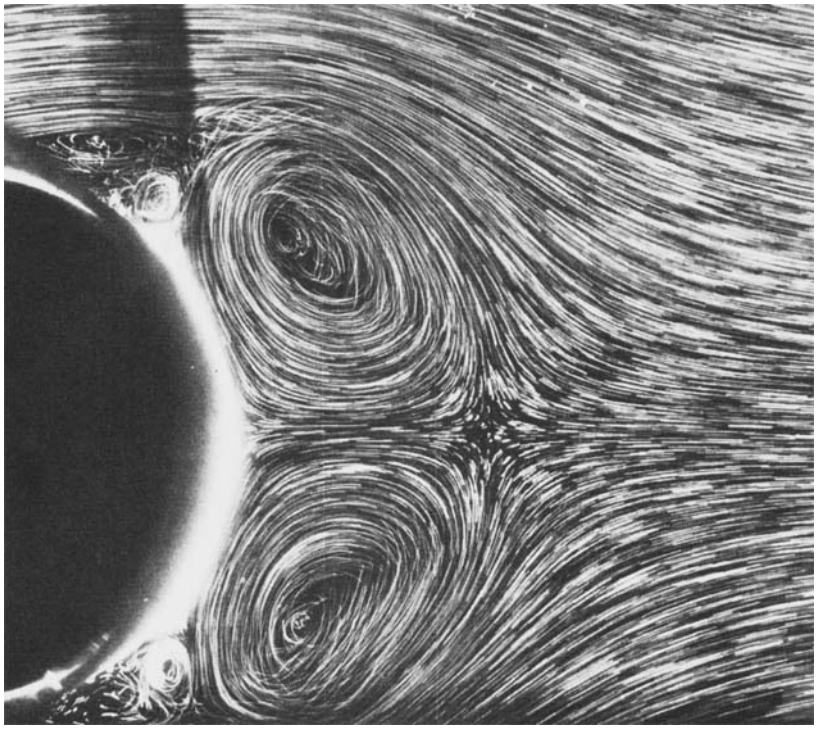

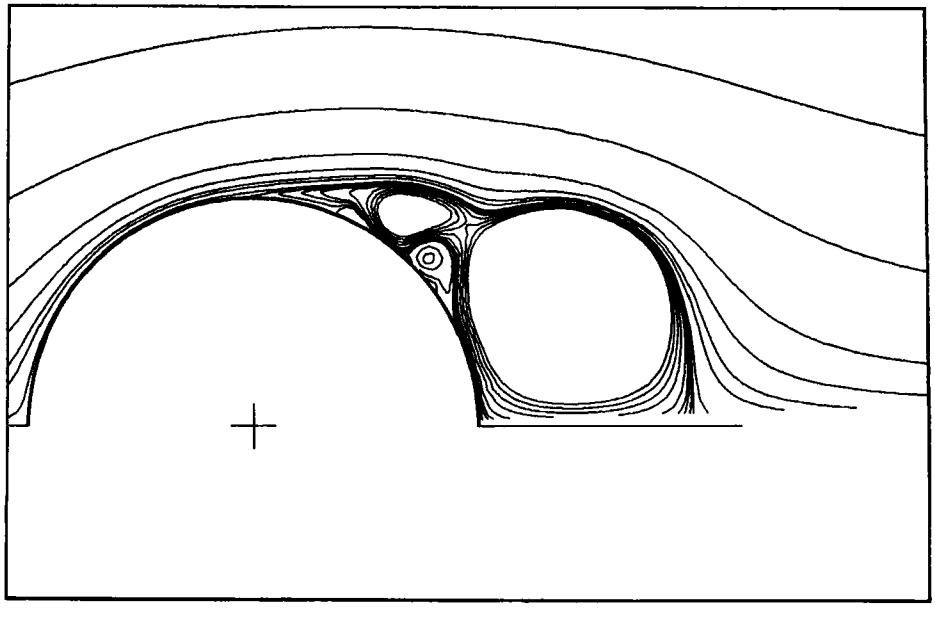

FIGURE 21. As figure 16; $t = 4$.

For the downstream boundary condition at infinity an open boundary condition has been established by assuming that the viscous-diffusive effect is negligible; the transport terms of the vorticity equation are then the only ones retained:

$$\left| g(\xi, \eta)\frac{\partial \omega}{\partial t} + \frac{\partial}{\partial \eta}\left(\frac{\partial \psi}{\partial \xi}\omega\right) - \frac{\partial}{\partial \xi}\left(\frac{\partial \psi}{\partial \eta}\omega\right)\right|_{\xi = \xi_\infty} = 0.$$

This condition is similar to the so-called 'radiant Sommerfeld condition'. With a one-side-discretized formula, this condition can be written as

$$\begin{aligned} & g(\xi_\infty, \eta_0)\frac{\omega^{n+1}(\xi_\infty, \eta_0) - \omega^n(\xi_\infty, \eta_0)}{2\Delta t} \\ & + \frac{1}{2\Delta \eta}\left[\frac{\partial \psi}{\partial \xi}(\xi_\infty, \eta_0 + \Delta\eta)\,\omega^n(\xi_\infty, \eta_0 + \Delta\eta) - \frac{\partial \psi}{\partial \xi}(\xi_\infty, \eta_0 - \Delta\eta)\,\omega^n(\xi_\infty, \eta_0 - \Delta\eta)\right] \\ & - \frac{1}{\Delta \xi}\left[\frac{\partial \psi}{\partial \eta}(\xi_\infty, \eta_0)\,\frac{\omega^{n+1}(\xi_\infty, \eta_0) + \omega^{n-1}(\xi_\infty, \eta_0)}{2}\right. \\ & \left. - \frac{\partial \psi}{\partial \eta}(\xi_\infty - \Delta\xi, \eta_0)\,\omega^n(\xi_\infty - \Delta\xi, \eta_0)\right] = 0, \end{aligned}$$

where $n+1$, n, $n-1$ represent the time index. This open boundary condition permits the effect of reflection to be reduced. A theoretical analysis of the reflection characteristics is not possible for the general case.

Calculations carried out with the irrotational-flow boundary condition and the open boundary condition on the downstream side have shown the efficiency of the latter: the domain of computation can be limited to about five radii of the circular cylinder without causing perturbations on the formation of the vortices.

The vorticity distribution at the surface of the cylinder is shown in figure 10. The appearance of the peaks of vorticity and a multiplication of secondary vortices may be noticed. The evolution with time of the radial velocity, behind the cylinder, on the axis of symmetry is compared with the experimental data in figure 11, and this comparison is found to be satisfactory. The influence of the mesh size and of the domain of computation on the flow structure induces a slight variation, as shown in figures 12 (*a*, *b*) at $t = 2$. The development of the flow pattern with time is presented in figures 13 and 14 for a grid system of 101×301 nodes, and a domain of computation limited by $r_\infty = 5$ and $0 \leqslant \theta \leqslant \pi$. The dimensionless time step is equal to 0.02. The main unsteady wake length behind the cylinder, measured experimentally and determined by numerical simulation, is shown in figure 15, and confirms a good degree of quantitative comparison. In figures 16–21 a comparison between experimental visualization and numerical results for the flow structure is shown; there is good agreement. The phenomenon β, observed experimentally, can be seen for all grid systems. The secondary vortices interact alternatively with the external flow and the main wake (figure 14, $t = 3.6$; figure 18, $t = 2$).

5. Conclusion

Results reported in this paper demonstrate that a correct numerical solution of the unsteady Navier–Stokes equations is a good way to simulate the time evolution of viscous flow around a circular cylinder for Reynolds numbers up to 10^4.

The efficiency of the high-order numerical scheme used in this paper is confirmed, and we hope to use it for greater Reynolds numbers.

Phenomena α and β detected in experimental visualization have been reproduced in detail by numerical simulation. The phenomenon of iteration between the external main flow and the secondary vortices has been pointed out for the first time, as shown in figure 14, $t = 3.6$, and figure 18, $t = 2$.

The increase of Reynolds number involves the multiplication of secondary vortices and the existence of a peak of vorticity at the surface of the cylinder, inside the separation area.

REFERENCES

BLASIUS, H. 1908 Grenzschichten in Flüssigkeiten mit kleiner Reibung. *Z. angew. Math. Phys.* **56**, 1.

BOUARD, R. & COUTANCEAU, M. 1980 The early stage of development of the wake behind an impulsively started cylinder for $40 < Re < 10^4$. *J. Fluid Mech.* **101**, 583.

COLLINS, W. M. & DENNIS, S. C. R. 1973*a* The initial flow past an impulsively started circular cylinder. *Q. J. Mech. Appl. Maths* **26**, 53.

COLLINS, W. M. & DENNIS, S. C. A. 1973*b* Flow past an impulsively started circular cylinder. *J. Fluid Mech.* **60**, 105.

COUTANCEAU, M. & BOUARD, R. 1977 Experimental determination of the main features of the viscous flow in the wake of a circular cylinder in uniform translation. Part 2. Unsteady flow. *J. Fluid Mech.* **79**, 257.

COUTANCEAU, M. & BOUARD, R. 1979 Sur la formation de tourbillons secondaires dans le sillage d'un cylindre soumis à un départ impulsif. *C.R. Acad. Sci. Paris* **288**, B45.

DAUBE, O. & TA PHUOC LOC 1978 Etude numérique d'écoulements instationnaires de fluide visqueux incompressible autour de corps profile par une méthode combinée d'ordre $O(h^2)$, $O(h^4)$. *J. Méc.* **17**, 651.

DENNIS, S. C. R. & STANIFORTH, A. N. 1971 A numerical method for calculating the initial flow past a cylinder in a viscous fluid. In *Proc. 2nd Intl Conf. on Numerical Methods in Fluid Dynamics* (ed. M. Holt). Lecture Notes in Physics, vol. 8, p. 343. Springer.

GOLDSTEIN, S. & ROSENHEAD, L. 1936 Boundary layer growth. *Proc. Camb. Phil. Soc.* **32**, 392.

HONJI, H. & TANEDA, S. 1969 Unsteady flow past a circular cylinder. *J. Phys. Soc. Japan* **27**, 1968.

INGHAM, D. B. 1968 Note on the numerical solution for unsteady viscous flow past a circular cylinder. *J. Fluid Mech.* **31**, 815.

JAIN, P. C. & RAO, K. S. 1969 Numerical solution of unsteady viscous incompressible fluid flow past a circular cylinder. *Phys. Fluids Suppl.* **12**, II-57.

KAWAGUTI, M. & JAIN, P. C. 1966 Numerical study of a viscous fluid past a circular cylinder. *J. Phys. Soc. Japan* **21**, 2055.

MONNET, P., COUTANCEAU, M., DAUBE, O. & TA PHUOC LOC 1983 The use of visualization as a guide in the numerical determination of the flow around an abruptly accelerated elliptic cylinder or airfoil. In *Proc. 3rd Intl Symp. on Flow Visualization, Ann Arbor.*

ORSZAG, S. A. & ISRAELI, M. 1974 Numerical simulation of viscous fluid flow. *Ann. Rev. Fluid Mech.* **6**, 281.

PATEL, V. A. 1976 Time dependent solutions of the viscous incompressible flow past a circular cylinder. *Comp. Fluids* **4**, 13.

PAYNE, R. B. 1958 Calculations of unsteady viscous flow past a circular cylinder. *J. Fluid Mech.* **4**, 81.

SCHUH, H. 1953 Calculation of unsteady boundary layers in two dimensional laminar flow. *Z. Flugwiss.* **1**, 122.

SON, J. S. & HANRATTY, T. J. 1969 Numerical solution of the flow around a cylinder at Reynolds number of 40, 200, 500. *J. Fluid Mech.* **35**, 369.

TANEDA, S. 1972 Visualization experiments on unsteady viscous flows around cylinders and plates. In *Recent Research on Unsteady Boundary Layers*, vol. 2 (ed. E. A. Eichelbrenner). Quebec Laval University.

TA PHUOC LOC 1980 Numerical analysis of unsteady secondary vortices generated by an impulsively started circular cylinder. *J. Fluid Mech.* **100**, 111.

THOM, A. 1933 The flow past circular cylinders at low speeds. *Proc. R. Soc. Lond.* A **141**, 651.

THOMAN, D. C. & SZEWCZYK, A. A. 1969 Time dependent viscous flow over a circular cylinder. *Phys. Fluids Suppl.* **12**, II-76.

WANG, C. Y. 1967 The flow past a circular cylinder which is started impulsively from rest. *J. Maths & Phys.* **46**, 195.

WATSON, E. J. 1955 Boundary layer growth. *Proc. R. Soc. Lond.* A **231**, 104.

WUNDT, H. 1955 Wachstum der laminaren Grenzschicht an schräg angeströmten Zylindern bei Anfahrt aus der Ruhe. *Ing.-Arch. Berlin* **23**, 212.